Magnesium Sulfate Aerosols Studied by FTIR Spectroscopy: Hygroscopic Properties, Supersaturated Structures, and Implications for Seawater Aerosols

Li-Jun Zhao, Yun-Hong Zhang,* Zun-Feng Wei, Hua Cheng, and Xiao-Hong Li

The Institute for Chemical Physics, Beijing Institute of Technology, Beijing 100081, People's Republic of China

Received: September 18, 2005; In Final Form: November 23, 2005

Supersaturated $MgSO_4$ aerosols and dilute $MgSO_4$ solutions were studied by FTIR spectroscopic techniques (i.e., aerosol flow tube (AFT) and attenuated total reflection (ATR)). The hygroscopic properties of $MgSO_4$ aerosols were investigated with results in good agreement with previous measurements by a scanning electrodynamic balance (SEDB). Well-defined spectral evolutions with changing relative humidity (RH) for the υ_3 band of SO_4^{2-} and the water O−H stretching envelope could be directly related to the observed hygroscopic properties of $MgSO_4$ aerosols. When the RH decreased from ∼55 to ∼40%, the υ_1 band of SO_4^{2-} in supersaturated $MgSO_4$ aerosols was observed to transform from a sharp peak at ∼983 cm^{-1} into a wide band at ∼1005 cm^{-1}. The sharp peak at ∼983 cm^{-1} was mainly assigned to such associated complexes of Mg^{2+} and SO_4^{2-} as double solvent-separated ion pairs (2SIPs), solvent-shared ion pairs (SIPs), and simple contact ion pairs (CIPs) in supersaturated $MgSO_4$ aerosols, while the wide band at ∼1005 cm^{-1} was due to polymeric CIPs chains, probably the main component of gels formed in $MgSO_4$ aerosols at low RHs. Relating to this υ_1 band transformation, the peak position of the υ_3 band was first shown to be a sensitive indicator of CIPs formation, spanning across ∼40 cm^{-1} on the formation of polymeric CIPs chains, which could also be supported by aerosol composition analysis in the form of water-to-solute molar ratios (WSR). In the water O−H stretching envelope, the absorbance intensities at 3371 and 3251 cm^{-1} were selected to represent contributions from weak and strong hydrogen bonds, respectively. The absorbance intensity ratio changing with RH of 3371 to 3251 cm^{-1} could be related to the previous observations with the υ_1 and υ_3 bands of SO_4^{2-}. As a result, the formation of CIPs with various structures in large amounts was supposed to significantly weaken hydrogen bonds in supersaturated $MgSO_4$ aerosols, while 2SIPs and SIPs were not expected to have similar effects even when occurring in abundance. In comparison with $MgSO_4$ aerosols, the peak positions of the υ_3 band of SO_4^{2-} in artificial seawater aerosols implied that the $MgSO_4$ component should be contained as gels or concentrated solutions in the fissures of microcrystals of sea salts for freshly formed seawater aerosols at low RHs.

Introduction

Seawater is rich in cations and anions of many types, among which Mg^{2+} and SO_4^{2-} are the most abundant except Na^+ and Cl^-, followed in turn by Ca^{2+}, K^+, HCO_3^-, Br^-, Sr^{2+} and so on in rapidly decreasing amounts.[1,2] According to some estimations, about 10^{12} to 10^{13} kg of sea salts is annually injected into the atmosphere in the form of seawater aerosols.[3−5] Besides the huge reservoir of seawater where it is responsible for the high absorption of sound,[6−9] $MgSO_4$ is also present in many natural brines.[10] Despite the similarities of the hygroscopic properties of NaCl and seawater aerosols,[2] sea salt particles with hollow structures have been observed to form from evaporation of seawater aerosols by a scanning electron microscope (SEM),[11] rather than the proposed structures III or IV for effloresced NaCl aerosol particles.[3] The morphologies of seawater aerosols at low RHs need to be further investigated on the molecular level by vibrational spectroscopy (i.e., Raman and/or infrared spectroscopy). Without the knowledge of aerosol morphologies, particle sizes obtained from light scattering techniques, which may fall into error by themselves,[12] cannot be directly converted to particle masses. An appropriate sea salt whose vibrations are sensitive to microenvironments may be used to follow the evaporation and condensation of seawater aerosols undergoing a water cycle. Actually, SO_4^{2-} is the only anion that can be practically used to characterize freshly formed seawater aerosols, and Mg^{2+} is much more qualified than Na^+ and other cations in seawater for that purpose because the interactions between Na^+ and SO_4^{2-} have no significant effect on the vibrations of SO_4^{2-} even in supersaturated Na_2SO_4 aerosols,[13] and other cations such as Ca^{2+}, K^+, and Sr^{2+} are in considerably smaller amounts than Mg^{2+}. With the spectral features of $MgSO_4$ aerosols being clearly identified and correctly understood, important deductions may be made about the morphologies of seawater aerosols at low relative humidities (RHs).

Few studies of the hygroscopic properties of $MgSO_4$ aerosols seem to have been made in the past several decades before 1998, except the two investigations made by Charlson et al. using an integrating nephelometer in 1978[14] and by Tang et al. using an electrodynamic balance (EDB) in 1997.[2] Since then, a series of work concerning $MgSO_4$ aerosols has been reported by a group of researchers.[13,15−20] For example, Chan et al. have made some EDB measurements of $MgSO_4$ aerosol droplets in 1998 and suggested that $MgSO_4$ aerosols form gels at low RHs.[15] Not

* Corresponding author. E-mail: yhz@bit.edu.cn; phone: 86-10-6891 2652; fax: 86-10-6891 2652.

10.1021/jp055291i CCC: $33.50
Published on Web 01/04/2006

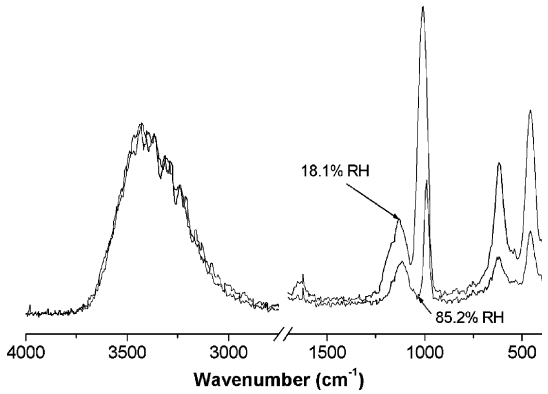

Figure 1. Raman spectra of highly concentrated (18.1% RH) and relatively dilute (85.2% RH) droplets of $MgSO_4$ aerosols. After normalization, the water O−H stretching envelopes in these two droplets are indistinguishable from each other due to morphology-dependent resonances (MDRs).

long after this, an even more detailed EDB investigation of $MgSO_4$ aerosols was given.[16] The water activity study of the aerosols of sodium and magnesium salts proved that the mixture of Na_2SO_4 and $MgSO_4$ (1:1) has a lower evaporation rate than other mixtures under investigation due to the presence of $MgSO_4$, and the structure involving hydrate and gel formation was proposed for the mixture at low RHs.[17] The gels formed in the previous aerosol systems (i.e., $MgSO_4$ and the mixture of Na_2SO_4 and $MgSO_4$ (1:1)) were further investigated and verified by two subsequent EDB investigations enhanced by Raman spectroscopy.[13,18] The formation of polymeric contact ion pairs (CIPs) chains, probably the main component of gels at low RHs, was believed to cause the observed mass transfer limitations.[13,18] More recently, one hygroscopic growth curve of a single dried (at ~10% RH) $MgSO_4$ aerosol particle has been drawn by taking advantage of a so-called scanning EDB (SEDB), disclosing the presence of serious mass transfer limitations at low RHs.[19] Furthermore, recent ab initio calculations also presented theoretical results consistent with the formation of long CIPs chains in supersaturated $MgSO_4$ aerosols.[20] Thus, the formation of gels in these aerosol systems involving $MgSO_4$ at low RHs has been reliably established, and the first Raman investigations were performed to understand supersaturated $MgSO_4$ aerosols on the molecular level.

Raman and Fourier transform infrared (FTIR) spectroscopies are complementary in the observation of molecular vibrations. Up to now, only Raman spectroscopy has been used in the previous EDB investigations; therefore, our knowledge about the spectral features of $MgSO_4$ aerosols is still very limited. As shown in Figure 1, in the normalized Raman spectra of highly concentrated (18.1% RH) and relatively dilute (85.2% RH) droplets of $MgSO_4$ aerosols, the water O−H stretching envelopes are actually indistinguishable from each other due to morphology-dependent resonances (MDRs).[13,18] Moreover, in previous Raman investigations of $MgSO_4$ aerosols, discussions have focused mainly on the Raman active υ_1 vibration of SO_4^{2-}, while the infrared active υ_3 vibration only presented a weak band in Raman spectra and could not be used to analyze supersaturated structures in $MgSO_4$ aerosols.[13,18] Considering the previous facts, it is timely to make some FTIR spectroscopic investigations of supersaturated $MgSO_4$ aerosols.

In a study of atmospheric aerosols, a FTIR spectrometer and an aerosol flow tube (AFT) can be assembled into a widely used FTIR/AFT system.[21] For example, Cziczo et al. have used a FTIR/AFT in the research of tropospheric aerosols a few years ago (1997)[22] and observed a considerable red shift for the υ_3 band of SO_4^{2-} with increasing RH in artificial seawater aerosols. However, no efforts were made then to understand what should be responsible for this red shift. By comparison with the results from our FTIR spectroscopic investigations of $MgSO_4$ aerosols performed in this work, the spectral features of SO_4^{2-}, especially the υ_3 band in artificial seawater aerosols, are believed to have important implications. The successful construction of a continuous sampling FTIR/AFT in our previous work has enabled us to carry out FTIR spectroscopic investigations of $MgSO_4$ aerosols.[23]

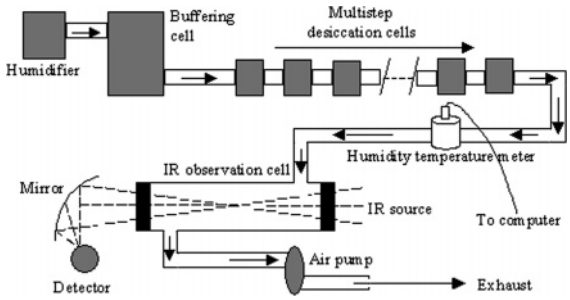

Figure 2. Schematic diagram of the continuous sampling FTIR/AFT (aerosol flow tube).

Experimental Procedures

Continuous Sampling FTIR/AFT for the Observation of $MgSO_4$ Aerosols. The continuous sampling FTIR/AFT has been constructed in an attempt to carry out FTIR spectroscopic investigations of supersaturated aerosols.[23] The setup is schematically shown in Figure 2, and its features will be briefly discussed together with measuring procedures to shed enough light on our experiments. Generally, the AFT used here is composed of an aerosol generator (ultrasonic humidifier), a buffering cell, multistep desiccation cells, an infrared (IR) observation cell, a humidity temperature meter (±2.5% RH, type CENTER 313), and an air pump.

$MgSO_4$ aerosols ranging from 1 to 5 μm in diameter were generated from dilute solutions of ~0.5 mol L^{-1} (prepared with triply distilled water and magnesium sulfate of analytical reagent grade) by the ultrasonic humidifier operated at room temperature (~18 °C) and under normal pressure. After that, under the guidance of the air pump, the aerosols flowed in turn through the buffering cell and the multistep desiccation cells (with color-changing silica gel desiccant placed inside) and then into the IR observation cell (18.5 cm in length, 5.5 cm in diameter) with silicon windows. Because of weakening drying ability of the desiccant with time, after passing through the multistep desiccation cells, the air flow bearing aerosol particles steadily increased in its RH, which was evident from the plot of RH versus time (not shown) recorded by the humidity temperature meter connected to a computer. By making use of the IR observation cell, this process could be continuously followed by a FTIR spectrometer (Nicolet Magna-IR 560). In measurements, a mercury cadmium telluride type A (MCT/A) detector cooled by liquid nitrogen was used. Totally, 32 scans were accumulated for the production of aerosol infrared spectra in the range of 4000−650 cm^{-1} and with a resolution of 4 cm^{-1}. The previous process has been defined as a reversed desiccation process and can be related to the reverse observation of ongoing dehumidifying processes of aerosols accompanying decreasing RH.[23a] Aerosol efflorescence should be available in the previous observation if it exists in the investigated RH range. Similarly, pure water was also used to generate aerosols. The humid air flow after passing through the multistep desiccation cells steadily

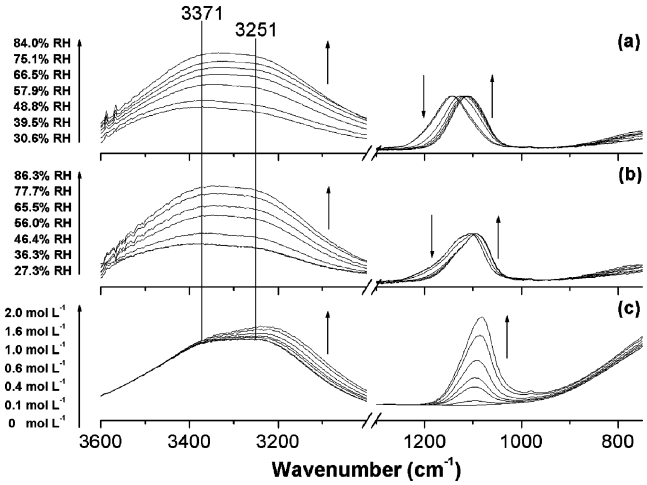

Figure 3. Infrared spectra of supersaturated $MgSO_4$ aerosols have been normalized to the υ_3 band of SO_4^{2-}, corresponding (a) to the reversed desiccation process and (b) to the humidifying process. The ATR spectra of dilute $MgSO_4$ solutions are shown in spectra c without normalization. Because no noticeable water-absorbing occurs below ~42.3% RH in the humidifying process, the spectra at 27.3 and 36.3% RH are essentially the same; thus only six spectra are visible in spectra b.

increased in its RH and was used to continuously humidify aerosol particles deposited in advance on the silicon windows of the IR observation cell. The hygroscopic growth of aerosols with increasing RH (and aerosol deliquescence at times) can thus be observed.

The validity of the continuous sampling FTIR/AFT method has just been discussed at length elsewhere[23b] and, therefore, will not be given in detail here. Comparisons between continuous sampling FTIR/AFT and SEDB measurements will be made at appropriate length in the first section of the Results and Discussion. The selected infrared spectra representing the reversed desiccation process and the humidifying processes are shown in Figure 3a,b, respectively. These spectra have been normalized to the υ_3 band of SO_4^{2-}, due to a number fluctuation of aerosol particles in the unit volume in the reversed desiccation process.

FTIR/ATR Measurements. The dilute $MgSO_4$ solutions of 0, 0.1, 0.4, 0.6, 1.0, 1.6, and 2.0 mol L^{-1} were prepared with the same solute and solvent as in the first section of the Experimental Procedures. The ATR spectra were collected at a room temperature of ~18 °C, using a baseline horizontal ATR cell (Spectra-Tech Inc.) equipped with a ZnSe crystal internal reflection element (IRE), intended for comparisons with the infrared spectra of supersaturated $MgSO_4$ aerosols. The dimensions of the ZnSe crystal IRE are 5×48 and 5×52 mm^2 with respect to the top small horizontal probe surface and the bottom large horizontal surface, respectively, and are 2 mm thick. The incident infrared beam is at an angle of 45° with respect to the top small horizontal probe surface, making about 12 internal reflections.[24] Instead of the MCT/A detector, a deuterated triglycine sulfate (DTGS) detector was used in the FTIR/ATR measurements, and altogether, 1024 scans were averaged to produce the desired ATR spectra in the range of 4000−750 cm^{-1} and with a resolution of 4 cm^{-1}. The ATR spectra of dilute $MgSO_4$ solutions are shown in Figure 3c without normalization.

Results and Discussion

Hygroscopic Properties of $MgSO_4$ Aerosols. As discussed previously, the reversed desiccation process can be related to the reverse observation of ongoing dehumidifying process, in

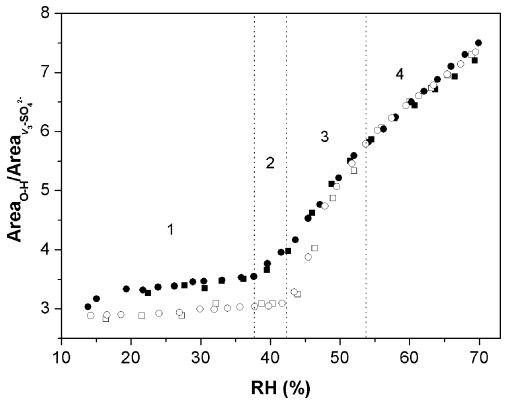

Figure 4. Hygroscopic properties of $MgSO_4$ aerosols, with filled circles and squares corresponding to the reversed desiccation process, while open circles and squares to the humidifying process. Circles and squares belong to independent measurements.

which aerosol droplets evaporate with decreasing RH, leading to potential aerosol efflorescence, while the humidifying process corresponds to the hygroscopic growth of aerosol particles with increasing RH, and aerosol deliquescence is potentially available in the observation. Therefore, it is possible to investigate the hygroscopic properties of $MgSO_4$ aerosols through the analysis of the infrared spectra collected in the previous two processes. The area ratio of the water O−H stretching envelope to the υ_3 band of SO_4^{2-} is the relative water content of $MgSO_4$ aerosols (briefly referred to as water content in the following discussion), and its change with RH actually reflects the hygroscopic properties of $MgSO_4$ aerosols. The selected region for the water O−H stretching envelope is 3550−2800 cm^{-1}, and that for the υ_3 band of SO_4^{2-} is 1299−950 cm^{-1}. Corrected baselines have been used in peak area calculations because a sloping background toward a high wavenumber due to Mie scattering has to be subtracted. The hygroscopic properties of $MgSO_4$ aerosols as investigated in the previous two processes are shown in Figure 4. The equilibrium RH of saturated $MgSO_4$ solutions at 25 °C is ~86%.[16]

The initial state of an investigated single particle in the humidifying process in SEDB measurements has been set at ~10% RH through evaporation,[19] very close to the ~12% RH in our continuous sampling FTIR/AFT measurements. The hygroscopic properties of $MgSO_4$ aerosols investigated by FTIR/AFT are generally very similar to those by the SEDB (see Figure 5 in ref 19), despite the fact that a different expression in the form of a mass fraction of solute (mfs) has been used in SEDB results. For a convenient explanation, Figure 4 is divided into four regions, which are region 1 (below ~37.8% RH), region 2 (~37.8 to ~42.3% RH), region 3 (~42.3 to ~53.7% RH), and region 4 (above ~53.7% RH), respectively. In region 1, the relatively constant water contents can be found in the two processes, and the water content in the reversed desiccation process is always higher than in the humidifying process above ~14% RH, at which point the water contents in the two processes become nearly equal. In region 2, aerosol particles in the humidifying process contain much less water than do those in the reversed desiccation process and show no sign of water-absorbing with increasing RH. This is due to the mass transfer limitations caused by the formation of gels at ~12% RH in the humidifying process. In contrast, the water content in the reversed desiccation process responds sensitively to changing RH, and no serious mass transfer limitations should be expected.[19] In region 3, although the water content in the reversed desiccation process and that in the humidifying process both respond very sensitively to changing RH, the slope is much

steeper in the humidifying process. Gels formed at ~12% RH on the silicon windows in the humidifying process begin to be dissolved with increasing RH through taking up water from an ambient environment, and at the upper limit of the region, the aerosol particle composition achieves equilibrium with ambient RH. In region 4, the equilibrium of aerosol particle composition with ambient RH can always be obtained in the humidifying process. The water contents in the two processes become accordingly equal and respond less sensitively to changing RH as compared with region 3. Although data points in SEDB results are not enough for us to make some detailed comparisons (especially in regions 1 and 2), throughout all regions, the same trend has been observed in continuous sampling FTIR/AFT and SEDB measurements.[19]

In SEDB measurements, a single levitated particle has been subject to an ambient environment with steadily changing RH. With the balancing voltage against particle gravity changing with the RH being measured simultaneously, aerosol compositions at different RHs can be determined by referring to the balancing voltage at a certain RH with a known composition.[19] For $MgSO_4$ aerosols, a rough calculation assuming a constant density produces completely dry aerosol particles of ~0.4 μm even for original aerosol droplets with a concentration of 0.5 mol L^{-1} and a lower limit of 1 μm. This means that the Kelvin effect is negligible in our experiments.[23b] While the flow rate and the volume of the pipeline system (between the multistep desiccation cells and IR observation cell) combined to allow ~6 s for aerosol particles (both pure water and aqueous $MgSO_4$ droplets) and air flow (i.e., ambient environment) to achieve equilibrium before entering the IR observation cell, the required time of about 1.25 h for one run of measurement was very comparable with previous SEDB measurements.[19] In addition to the detailed discussion made recently about the validity of the continuous sampling FTIR/AFT,[23b] the general good agreement between these two kinds of measurements on the hygroscopic properties of $MgSO_4$ aerosols has provided further experimental evidence on the capability of the continuous sampling FTIR/AFT.

The division of Figure 4 into the previous four regions will help to elucidate relevant spectral features, which are closely associated with the hygroscopic properties of $MgSO_4$ aerosols. In the following sections, detailed discussions will be made on the υ_1 and υ_3 bands of SO_4^{2-} and the water O−H stretching envelope in supersaturated $MgSO_4$ aerosols.

υ_1 and υ_3 Bands of SO_4^{2-} in Supersaturated $MgSO_4$ Aerosols. Aqueous $(NH_4)_2SO_4$ solutions have been considered as a model of free (unassociated) SO_4^{2-} systems.[10,13,18,24−26] Free SO_4^{2-} is of T_d symmetry as optimized by an ab initio investigation,[27] and its vibrations are all Raman active.[18,27] In the Raman spectra of dilute solutions of $(NH_4)_2SO_4$ aerosols at high RHs, the vibrations of SO_4^{2-} were found to give rise to four bands at ~981 (υ_1), ~463 (υ_2), ~1095 (υ_3), and ~618 cm^{-1} (υ_4), respectively.[18] In contrast, only the υ_3 and υ_4 vibrations of free SO_4^{2-} are infrared active.

The υ_1 band of SO_4^{2-} has always been the focus of many Raman investigations of aqueous $MgSO_4$ solutions, and its transformations could be used to indicate the extent of ion association.[10,13,18,28] The developing asymmetry of the strong υ_1 band with increasing concentration has been well-established as the evidence of the formation of simple CIPs in aqueous $MgSO_4$ solutions through recent research advances.[10,13,18] Rudolph et al.[10] further suggested that, in comparison with $(NH_4)_2SO_4$ solutions, the systematic difference of one component at ~980 cm^{-1} of the asymmetrical υ_1 band after subtraction of another component at ~993 cm^{-1} (simple CIPs) actually comes from the effect of solvent-shared ion pairs (SIPs) formed in dilute $MgSO_4$ solutions. Consistent with those Raman investigations, recent dielectric relaxation spectroscopy (DRS) studies also confirmed the existence of double solvent-separated ion pairs (2SIPs), SIPs, simple CIPs, and a triple ion $[Mg_2SO_4]^{2+}$ or possibly a more aggregated species in aqueous $MgSO_4$ solutions.[29] In a more recent confocal Raman study, CIPs with various structures have been observed to form roughly in steps with increasing concentration through the analysis of the υ_1 band of SO_4^{2-} in supersaturated $MgSO_4$ droplets.[30]

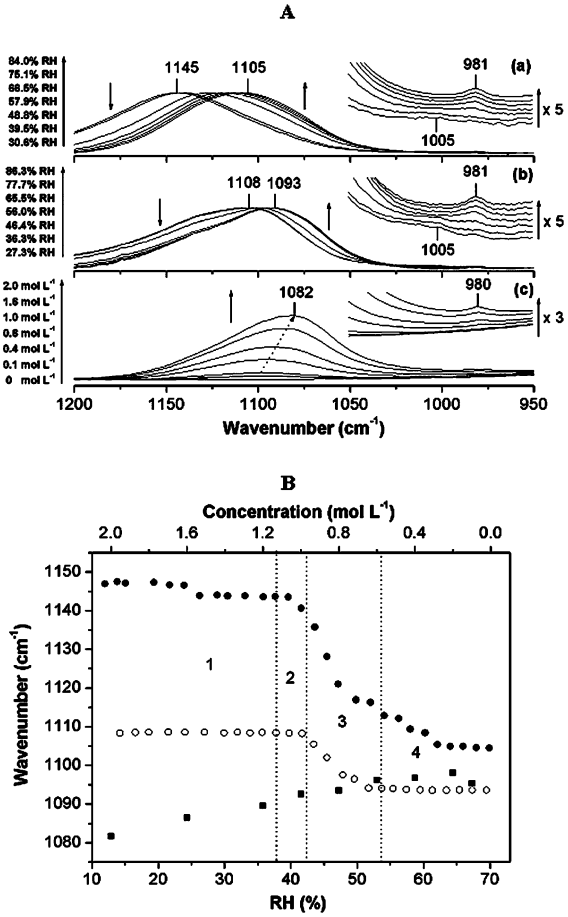

Figure 5. (A) υ_1 (shown on the top right of spectra a and b with a magnification of 5) and υ_3 bands of SO_4^{2-} are observed in the infrared spectra (normalized to the υ_3 band of SO_4^{2-}) of supersaturated $MgSO_4$ aerosols, corresponding (a) to the reversed desiccation process and (b) to the humidifying process. The above features (with the υ_1 band shown on the top right of spectra c with magnification of 3) can also be observed in the ATR spectra of dilute $MgSO_4$ solutions shown in spectra c without normalization. (B) Plot of the peak position of the υ_3 band of SO_4^{2-} vs RH (bottom *x* axis) and concentration (top *x* axis), in which filled circles, open circles, and filled squares correspond to the reversed desiccation process, the humidifying process, and the FTIR/ATR measurements, respectively.

According to spectra a and b in Figure 5A, a distinct band at ~983 cm^{-1} with narrow full width at half-height (fwhh) emerges in the infrared spectra of $MgSO_4$ aerosols collected above ~55% RH in the two processes. The band shifts slightly to a lower wavenumber (~981 cm^{-1}) with increasing RH, which corresponds to less concentrated solutions. As shown in spectra c of Figure 5A, in the ATR spectra of dilute $MgSO_4$ solutions, a faint band at ~978 cm^{-1} presents itself in the solution of ~0.4 mol L^{-1}, and the band continues to grow in intensity up to the concentration of 2 mol L^{-1}, shifting slightly at the same time to a higher wavenumber (~980 cm^{-1}). Although the υ_1 vibration

of free SO_4^{2-} is infrared inactive, the υ_1 band has been observed in the infrared spectra in both FTIR/AFT and FTIR/ATR measurements. Possible sources of the infrared activity of the υ_1 vibration of SO_4^{2-} are considered as follows. First, the symmetry reduction of SO_4^{2-} caused by the formation of simple CIPs should definitely bring about infrared activity for the υ_1 vibration.[24-26] Second, other factors, such as the formation of 2SIPs, SIPs, and even the solvent water itself, may also cause the υ_1 vibration to be infrared active.[24] The water is also considered because four polar solvents including water were found capable of reducing the D_{3h} symmetry of isolated NO_3^- to C_{2v} or C_s symmetry.[31,32] Free ClO_4^- is of T_d symmetry like SO_4^{2-}, and in aqueous solutions, ClO_4^- has been regarded as one of least associating anions.[23b] Despite this fact, the υ_1 band of ClO_4^- could be observed in the infrared spectra of dilute $NaClO_4$ solutions.[23b] In recent FTIR/ATR investigations when a highly sensitive MCT/A detector was used, even aqueous $(NH_4)_2SO_4$ solutions as a model of free SO_4^{2-} systems could be detected for the υ_1 band of SO_4^{2-} with concentrations as low as 0.1 mol L^{-1}.[24] Primary results for several sulfate solutions have been obtained by FTIR spectroscopy a few years ago.[25,26] Since the υ_1 band of SO_4^{2-} was observed at 981 cm^{-1} in a 3.51 mol/kg $CdSO_4$ solution, but was not evident in a 0.9 mol/kg Na_2SO_4 solution,[25,26] we reason that a less sensitive detector than MCT/A should have been used. The υ_1 band is generally very weak in the infrared spectra of the supersaturated $MgSO_4$ aerosols above ~55% RH and of the dilute $MgSO_4$ solutions, making it impossible to differentiate between the band of spectroscopically indistinguishable 2SIPs, SIPs, and free (unassociated) SO_4^{2-}[10] and that of simple CIPs. Nevertheless, because dilute $MgSO_4$ solutions have been shown to be significantly associated,[10,29] therefore, 2SIPs, SIPs, and simple CIPs should combine to contribute mostly to the infrared activity of the υ_1 vibration of SO_4^{2-} in the supersaturated $MgSO_4$ aerosols above ~55% RH and in the dilute $MgSO_4$ solutions.

As can be seen in spectra a and b of Figure 5A, the RH range from ~55 to ~40% roughly corresponds to a transitional processes, in which the band centered at ~983 cm^{-1} is disappearing and a new wide band centered at ~1005 cm^{-1} is emerging with decreasing RH. Once the RH is below ~40% in FTIR/AFT measurements, then the wide band at ~1005 cm^{-1} can be defined in the infrared spectra. This feature has been documented in recent Raman literature, for which the formation of a triple ion $[Mg_2SO_4]^{2+}$ or polymeric CIPs chains has been proposed to account.[10,18] Especially, the formation of long CIPs chains has been supported by recent ab initio calculations.[20]

With regard to the infrared active υ_3 and υ_4 bands of SO_4^{2-}, only the υ_3 band has been carefully examined in this work. Both υ_2 and υ_4 bands are beyond the range of our spectra (i.e., 4000−650 cm^{-1}). The υ_3 band has tended to be neglected in Raman investigations of $MgSO_4$ solutions, probably due to its weak signal in Raman spectra.[10,13,18,28] In contrast, in some Raman and infrared spectroscopic investigations of $CdSO_4$ solutions,[25,26] the occurrence of a low frequency shoulder on the υ_3 band of SO_4^{2-} in Raman spectra and the shift and broadening of the υ_3 band of SO_4^{2-} in infrared spectra has been used to indicate the symmetry distortion of SO_4^{2-} through the formation of CIPs.

As shown in Figure 5B, the plot of the peak position of the υ_3 band of SO_4^{2-} versus RH is also divided into the same four regions as in Figure 4. The peak position of the υ_3 band in supersaturated $MgSO_4$ aerosols shifts from ~1145 to ~1105 cm^{-1} in the reversed desiccation process with decreasing concentration accompanying increasing RH and from ~1108 to ~1093 cm^{-1} in the humidifying process. The peak position of the υ_3 band in dilute $MgSO_4$ solutions shifts from ~1098 to ~1082 cm^{-1} as the concentration increases from 0.1 to 2 mol L^{-1}, mainly due to the effect of anomalous dispersion.[33,34]

The development of the υ_3 band of SO_4^{2-} with RH shown in Figure 5B can be easily related to the hygroscopic properties of $MgSO_4$ aerosols displayed in Figure 4. In region 1, both the reversed desiccation process and the humidifying process maintain rather constant υ_3 peak positions with changing RH of ~1145 and ~1108 cm^{-1}, respectively, as the reflection of the relatively constant water contents in the same region in the two processes shown in Figure 4. In region 2, the peak position of the υ_3 band begins to decline sharply with increasing RH in the reversed desiccation process as a result of the sensitive response of the water content to changing RH but remains at ~1108 cm^{-1} in the humidifying process in response to the constant water content. In region 3, the sharp decline of the peak position of the υ_3 band with increasing RH in the two processes is the reflection of the sensitive response of the water contents to changing RH. In region 4, the peak position of the υ_3 band declines less rapidly with increasing RH in the two processes, due to the relatively insensitive response of the water contents to changing RH in comparison with region 3.

The peak positions of the υ_3 band at various RHs in the humidifying process have been found to displace downward as a whole with respect to those in the reversed desiccation process, as shown in Figure 5B. Aggregation by immediate aerosol particles may have led to the formation of bigger particles on the silicon windows, on which Mie scattering acts differently from those particles in the reversed desiccation process. But the overall effect of Mie scattering on the infrared spectra of aerosols is to introduce a sloping background toward high wavenumber and is generally not expected to move the band so drastically. Therefore, surface interactions between aerosol particles and silicon windows may dominantly cause the υ_3 band of SO_4^{2-} in the humidifying process to displace from that in the reversed desiccation process. The concern with Mie scattering can be further dispelled by checking the infrared spectra of $(NH_4)_2SO_4$ aerosols. The formation of CIPs by NH_4^+ and SO_4^{2-} has already been shown to have little effect on the vibrations of SO_4^{2-} even in supersaturated $(NH_4)_2SO_4$ aerosols.[13,18] In fact, in the infrared spectra of $(NH_4)_2SO_4$ aerosols (not shown) collected in the reversed desiccation process, it can be found that the peak position of the υ_3 band shifts only slightly (less than 3 cm^{-1}) in the wide RH range from ~30 to ~80%, totally incomparable with the wide shift in supersaturated $MgSO_4$ aerosols. The efflorescence RH for $(NH_4)_2SO_4$ aerosols is ~33%, and the deliquescence RH is ~79%.[21,22]

Referring to spectra a and b of Figure 5A, it is also shown that, when the RH decreases from ~55 to ~40%, the peak position shift of the υ_3 band in the two processes roughly coincides with the transformation of the υ_1 band from the sharp peak at ~983 cm^{-1} into the wide envelope at ~1005 cm^{-1}. The aerosol compositions in the reversed desiccation process are expected to approximate equilibrium with ambient RHs when there are no serious mass transfer limitations, which is the case for $MgSO_4$ aerosols above ~37.8% RH.[19] According to the published data,[13,18] the water-to-solute molar ratio (WSR) of $MgSO_4$ aerosols drops continuously from ~8 to ~5 as the RH decreases from ~53.7 to ~37.8% (through regions 3 and 2). Once the WSR approaches 5, to meet the hexacoordinate requirement, all Mg^{2+} will have to be directly associated with SO_4^{2-} if only simple CIPs are considered. Therefore, the process through regions 3 and 2 should correspond to the rapid formation of enormous amounts of CIPs in supersaturated $MgSO_4$ aerosols,

leading eventually to the formation of gels (composed mainly of polymeric CIPs chains), causing serious mass transfer limitations in region 1. Both the evolution of the υ_1 band and the aerosol composition analysis suggest that the υ_3 band of SO_4^{2-} should be very sensitive to the formation of CIPs. In the humidifying process evident in Figure 5B, the sharp decline of the peak position of the υ_3 band with increasing RH in region 3 must be related to the rapid consumption of CIPs in $MgSO_4$ aerosols with decreasing concentration.

Through the previous analysis, it can be confidently concluded that the peak position of the υ_3 band of SO_4^{2-} is of high sensitivity to the formation of CIPs in supersaturated $MgSO_4$ aerosols, which gives rise to a span across ~40 cm^{-1} on the formation of polymeric CIPs chains.

Water O−H Stretching Envelope in Supersaturated $MgSO_4$ Aerosols. The water O−H stretching envelope has usually been ignored in Raman investigations of $MgSO_4$ solutions (i.e., for both dilute bulk solutions[10,28] and supersaturated aerosol solutions[13,18]). Analysis of the Raman spectra of supersaturated $MgSO_4$ aerosols is constantly hindered by the low quality of the spectra, which is largely attributed to morphology-dependent resonances (MDRs) complicating the view.[13,18] The water features have yet to be discussed on the formation of CIPs in supersaturated $MgSO_4$ aerosols.[13,18] At the same time, at least in two cases, the water O−H stretching envelope has been successfully used to extract information on supersaturated structures.[35,36] Recently, a theoretical study suggested that some of the water O−H stretching frequencies should red-shift up to 2000 cm^{-1} in a few hydrated magnesium sulfate salts.[37] Therefore, to better understand supersaturated structures present in $MgSO_4$ aerosols, the RH-dependent evolution of the water O−H stretching envelope needs to be carefully examined.

Hydrogen bond strength of water decreases with increasing wavenumber under the water O−H stretching envelope in pure water and aqueous solutions; therefore, the strength of the hydrogen bonds can be qualitatively considered in terms of the wavenumber.[35] Referring to Figure 3a,b, it can be roughly seen that the water O−H stretching envelope in supersaturated $MgSO_4$ aerosols is enhanced on the high wavenumber side with an increased concentration accompanying decreased RH. In contrast, according to Figure 3c, the water O−H stretching envelope in dilute $MgSO_4$ solutions is obviously enhanced on the low wavenumber side with an increased concentration. Mg^{2+} has a large charge-to-radius ratio and hence can be easily hydrated in aqueous solutions. Hydrated Mg^{2+} is well-known to be comprised of six water molecules in its inner sphere,[18] and the complex is of T_h symmetry as optimized by an ab initio investigation.[38] Interestingly, recent experimental studies have confirmed the existence of isomeric structures of $Mg^{2+}(H_2O)_6$ in the gas phase, but the exact nature of these isomers has yet to be clarified.[39] Mg^{2+} has a polarization effect on the first hydration layer of water molecules, and the hydrogen bonds between the first and second hydration layers are thus significantly strengthened by the polarization effect of Mg^{2+}.[40] SO_4^{2-} has been regarded as a structure-maker, forming hydrogen bonds with water molecules, but the hydrogen bonds between SO_4^{2-} and water molecules are slightly weaker than those between water molecules.[18,24,27] Since only Mg^{2+} is expected to noticeably strengthen hydrogen bonds in dilute $MgSO_4$ solutions, it should be the growing fraction of strong hydrogen bonds caused by increasing abundance of Mg^{2+} that leads to the enhancement of the low wavenumber side of the water O−H stretching envelope with an increased concentration in dilute $MgSO_4$ solutions.

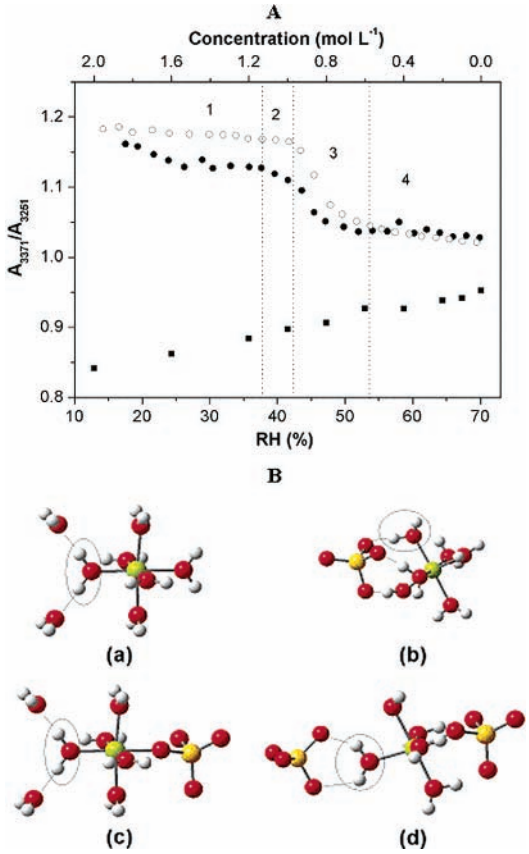

Figure 6. (A) Plot of the absorbance intensity ratio of 3371 to 3251 cm^{-1} vs RH (bottom *x* axis) and concentration (top *x* axis), in which filled circles, open circles, and filled squares correspond to the reversed desiccation process, the humidifying process, and the FTIR/ATR measurements, respectively. (B) Several representative species in supersaturated $MgSO_4$ aerosols. Gray, red, yellow, and green balls correspond to hydrogen, oxygen, sulfur, and magnesium atoms, respectively. The water molecules as hydrogen atom donors in hydrogen bonds are circled with thin lines for clarity.

To quantitatively understand the trend of the water O−H stretching envelope observed in supersaturated $MgSO_4$ aerosols, the absorbance intensities at 3371 and 3251 cm^{-1} have been selected to represent contributions from weak and strong hydrogen bonds, respectively. The corrected absorbance intensity has to be used to dispel the concern with Mie scattering. The absorbance intensity ratios of 3371−3251 cm^{-1} for selected spectra have been plotted against corresponding RHs, and the results are shown in Figure 6A, which is also divided into the same four regions as in Figure 4. The results can also be directly related to the hygroscopic properties of $MgSO_4$ aerosols shown in Figure 4. In region 1, generally, the higher water content in the reversed desiccation process corresponds to the lower fraction of weak hydrogen bonds than in the humidifying process, as shown in Figure 6A. In region 2, in contrast to the constant water content in the humidifying process, the water content in the reversed desiccation is very sensitive to changing RH, and the fact is reflected in Figure 6A as the constant hydrogen bond composition in the humidifying process and the sharp decline of the weak hydrogen bond fraction with an increased RH in the reversed desiccation process. In region 3, the water contents in the two processes are highly sensitive to changing RH, resulting in the rapid decline of the weak hydrogen bond fraction with an increased RH. In region 4, the water contents in the two processes are equal according to Figure

4, giving rise to the same hydrogen bond compositions. At the same time, referring to the previous discussions on the υ_1 and υ_3 bands of SO_4^{2-}, it has been shown that regions 1−3 can be related to the formation of CIPs with various structures in supersaturated $MgSO_4$ aerosols.

Through the previous correlation, it is very clear that the formation of various CIPs has led to the weakening of hydrogen bonds in supersaturated $MgSO_4$ aerosols. Although Mg^{2+} and SO_4^{2-} are both structure-makers, which strengthen hydrogen bonds or form hydrogen bonds with water molecules in dilute $MgSO_4$ solutions, the formation of CIPs by Mg^{2+} and SO_4^{2-} is thus shown to weaken hydrogen bonds in supersaturated $MgSO_4$ aerosols. Several representative species in the two processes are shown in Figure 6B, with the water molecules as hydrogen atom donors in hydrogen bonds being circled with thin lines for clarity. Because of the polarization effect of Mg^{2+}, the interactions between the first and the second hydration layers of water molecules are strong hydrogen bonds (e.g., with a structure like part a in Figure 6B). Because the hydrogen bonds between SO_4^{2-} and water molecules are only slightly weaker than those between water molecules, the formation of SIPs (and 2SIPs) (e.g., with a structure like part b in Figure 6B) is not expected to decrease the strong hydrogen bond fraction in an appreciable amount. Therefore, the rapid formation of various CIPs (e.g., with structures such as parts c and d in Figure 6B) should account for the sudden increase of weak hydrogen bond fraction with a decreased RH through regions 3 and 2 in the reversed desiccation process according to Figure 6A. Similarly, the rapid consumption of various CIPs should account for the sudden decrease of the weak hydrogen bond fraction with an increased RH through region 3 in the humidifying process according to Figure 6A. Structures for other more complex CIPs such as the triple ion $[Mg_2SO_4]^{2+}$ and long CIPs chains can be found elsewhere.[18,20,29]

Consistent with the previous qualitative discussions on the opposite trends of the water O−H stretching envelope with an increased concentration in supersaturated $MgSO_4$ aerosols and in dilute $MgSO_4$ solutions, according to Figure 6A, the absorbance intensity ratio of 3371−3251 cm^{-1} is on the rise with an increased concentration accompanying a decreased RH in supersaturated $MgSO_4$ aerosols, while on the decline with an increased concentration in dilute $MgSO_4$ solutions. Because FTIR/AFT and FTIR/ATR are very different technologies featuring inherent advantages and disadvantages, the apparent absorbance intensity ratios obtained by these two technologies may not be compared directly with each other.[33,34,41] Although seemingly contradictory, the previous observations can be rationalized as follows: the addition of more solute into dilute solutions of $MgSO_4$ causes an increase of a strong hydrogen bond fraction due to the polarization effect of Mg^{2+}, but as the concentration increases up to certain point of extreme supersaturation that can only be realized in aerosols, then the rapid formation of CIPs with various structures with increasing concentrations accompanying decreasing RH will remarkably decrease the fraction of strong hydrogen bonds in aqueous solutions.

Implications for Seawater Aerosols. Many cations and anions present in seawater are just blank ions for detection by vibrational spectroscopy (i.e., Raman and/or infrared spectroscopy) except only a few anions such as SO_4^{2-}. In addition, SO_4^{2-} can be further favored by its large amount in seawater. $MgSO_4$ aerosols have come under intensive investigation by FTIR spectroscopy in this work, primarily due to the pronounced effect of Mg^{2+} on the vibrations of SO_4^{2-}.[13,18]

From Figure 9 in ref 22, it can be clearly seen that the υ_3 band of SO_4^{2-} is the only prominent band in artificial seawater aerosols, except the water O−H stretching and bending envelopes. To advance discussions, the peak positions at various RHs (not clear in ref 22 but provided by Dr. Daniel J. Cziczo through personal correspondence) of the υ_3 band of SO_4^{2-} in the infrared spectra of submicron artificial seawater aerosols collected in a so-called deliquescence-mode experiment are given as follows: 1145 cm^{-1} when approaching zero RH, 1130 cm^{-1} at ∼5% RH, 1120 cm^{-1} at ∼25% RH, 1115 cm^{-1} at ∼50% RH, 1110 cm^{-1} at ∼75% RH, and 1100 cm^{-1} at ∼95% RH, and the reported RHs claimed an accuracy of ±1%.[22] For the simple reason of keeping the consistency of our figures in the RH range to promote general discussions with the features of $MgSO_4$ aerosols, we would rather give these data (with very different RH ranges) as stated previously than include them in Figure 5B. Because of the calculated and observed sequential formation of microcrystals from seawater solutions on evaporation,[42,43] various sea salts probably do not effloresce into a uniform solid. Therefore, the peak position at 1145 cm^{-1} of the υ_3 band of SO_4^{2-} may be related to $MgSO_4$ gels present as one of heterogeneous phases in seawater aerosols as the RH is lowered toward zero. The formation of $MgSO_4$ gels in seawater aerosols is accordingly expected to occur at much lower ambient RH (approaching zero) than observed in $MgSO_4$ aerosols (∼37.8% RH) in this work. To rationalize this fact, concentrated $MgSO_4$ solutions may be contained in the fissures of microcrystals of sea salts for seawater aerosols at low RHs. Since the surfaces of microcrystals are probably wetted by $MgSO_4$ solutions and due to the Kelvin effect, the much smaller water vapor partial pressure caused by the concave liquid surfaces at the exits of fissures, relative to the horizontal surface, probably has decreased the ambient RH at which $MgSO_4$ gels are expected to form from ∼37.8% in $MgSO_4$ aerosols to approaching zero in seawater aerosols. It is apparent that $MgSO_4$ gels contained in the fissures of microcrystals of sea salts already become dissolved at ∼5% RH as indicated by the peak position at 1130 cm^{-1}, in contrast to the ∼42.3% RH when $MgSO_4$ gels on the silicon windows in the humidifying process begin to be dissolved. According to the previous data, the peak position of the υ_3 band in artificial seawater aerosols declines rapidly with increasing RH. This should mean that, as ambient RH increases, $MgSO_4$ gels and concentrated $MgSO_4$ solutions contained in the fissures of microcrystals will be quickly dissolved and diluted through taking up water from the ambient environment.

The previous discussions agree well with the image of seawater aerosols at low RHs envisaged by Weis and Ewing,[44] who have argued that sea salt particles should be "internal mixtures of microcrystalline and amorphous regions of varying composition and shape with inclusions of aqueous salt solutions". Since $MgSO_4$ aerosols have such unique hygroscopic properties as discussed in this paper, the presence of significant amounts of $MgSO_4$ in seawater aerosols should contribute to the formation of hollow sea salt particles[11] (e.g., acting as a binding agent between microcrystals of sea salts at low RHs).

Although partially understood by the previous discussions, it should still be unambiguously pointed out that the basic facts for drawing the previous conclusions are just the peak positions of the υ_3 band of SO_4^{2-} in $MgSO_4$ and artificial seawater aerosols. Educated extrapolations have been made accordingly to give some implications for freshly formed seawater aerosols at low RHs. In addition to the previous explanations, other possibilities also may need to be considered. Seawater is a very complicated mixture of many cations and anions, and new matter

other than what is normally expected might form in seawater aerosols under different atmospheric conditions, whose influences on the υ_3 band of SO_4^{2-} might invalidate the previous conclusions to an uncertain extent. It will remain an open question, but for the time being, we just have no definite proof of new matter formation that can discredit the previous conclusions for freshly formed seawater aerosols at low RHs.

Conclusions

Supersaturated $MgSO_4$ aerosols and dilute $MgSO_4$ solutions have been studied by FTIR spectroscopy in this paper to obtain deep insight into the hygroscopic properties and supersaturated structures of $MgSO_4$ aerosols. With $MgSO_4$ as a probe molecule, some interesting implications have been made for freshly formed seawater aerosols at low RHs. According to our understanding, this work contributes several aspects as follows:

(1) In the infrared spectra of supersaturated $MgSO_4$ aerosols, the υ_1 band of SO_4^{2-} was observed to transform from a sharp peak at $\sim$983 cm^{-1} into a wide band at $\sim$1005 cm^{-1} when the RH decreased roughly from $\sim$55 to $\sim$40%. Relating to this υ_1 band transformation, and resorting to aerosol composition analysis in the form of water-to-solute molar ratio (WSR), the peak position of the υ_3 band of SO_4^{2-} was first shown to be highly sensitive to CIPs formation, and a wide shift of $\sim$40 cm^{-1} was found on the formation of polymeric CIPs chains.

(2) In addition to the υ_1 and υ_3 bands of SO_4^{2-}, the water O−H stretching envelope has also been found to be sensitive to the formation of CIPs. By correlating the change with RH of an absorbance intensity ratio of 3371−3251 cm^{-1} with the observations of the υ_1 and υ_3 bands of SO_4^{2-}, the formation of CIPs with various structures in large amounts was supposed to weaken hydrogen bonds in supersaturated $MgSO_4$ aerosols, while 2SIPs and SIPs were not expected to behave similarly.

(3) By extrapolating from $MgSO_4$ aerosols, the peak positions of the υ_3 band of SO_4^{2-} in artificial seawater aerosols suggested that the $MgSO_4$ component should be contained as gels or concentrated solutions in the fissures of microcrystals of sea salts for freshly formed seawater aerosols at low RHs, which were then quickly dissolved and diluted with increasing ambient RH through taking up water from the ambient environment.

According to the previous findings, subsequent research may be carried out to address the following problems concerning seawater aerosols. Because of their ability to form gels in aerosols at low RHs,[36,45,46] the potential roles of $NaNO_3$, $Mg(NO_3)_2$, $Ca(NO_3)_2$, and $Sr(NO_3)_2$ in aged seawater aerosols at low RHs may deserve some attentions. Since $MgSO_4$ has been found to be responsible for the high absorption of sound in seawater, which can be directly related to the distributions of various associated complexes of Mg^{2+} and SO_4^{2-},[6−9] we also suggest that some sound absorption measurements for seawater aerosols be made. Some characteristic patterns of sound absorption by seawater aerosols at different RHs may be found, which could be of potential applications in fields such as seawater aerosol characterization and maritime environment monitoring.

Acknowledgment. This work was supported by the National Natural Science Foundation of China (NSFC) through Grants 20073004 and 20473012, by the Trans-Century Training Program Foundation for the Talents of the Ministry of Education of China, and by the Incubation and Reward Foundation for Excellent Doctoral Dissertation of Beijing Institute of Technology. We are grateful to Dr. Daniel J. Cziczo for showing us the detailed υ_3 peak positions of SO_4^{2-} in the infrared spectra of artificial seawater aerosols.

References and Notes

(1) Kester, D. R.; Duedall, I. W.; Connors, D. N.; Pytkowicz, R. M. *Limnol. Oceanogr.* **1967**, *12*, 176.
(2) Tang, I. N.; Tridico, A. C.; Fung, K. H. *J. Geophys. Res.* **1997**, *102* (D19), 23269.
(3) Weis, D. D.; Ewing, G. E. *J. Geophys. Res.* **1999**, *104* (D17), 21257.
(4) Blanchard, D. C. *J. Geophys. Res.* **1985**, *90* (C1), 961.
(5) Cipriano, R. J.; Blanchard, D. C. *J. Geophys. Res.* **1981**, *86* (C9), 8085.
(6) Fisher, F. H. *J. Phys. Chem.* **1962**, *66*, 1607.
(7) Fisher, F. H. *Science* **1967**, *157*, 823.
(8) Fisher, F. H. *Geochim. Cosmochim. Acta* **1972**, *36*, 99.
(9) Hsu, C. C.; Fisher, F. H. *J. Acoust. Soc. Am.* **1983**, *74*, 564.
(10) Rudolph, W. W.; Irmer, G.; Hefter, G. T. *Phys. Chem. Chem. Phys.* **2003**, *5*, 5253.
(11) Cheng, R. J.; Blanchard D. C.; Cipriano, R. J. *Atmos. Res.* **1988**, *22*, 15.
(12) Pinnick, R. G.; Carroll, D. E.; Hofmann, D. J. *Appl. Opt.* **1976**, *15*, 384.
(13) Zhang, Y.-H.; Chan, C. K. *J. Phys. Chem. A* **2002**, *106*, 285.
(14) Charlson, R. J.; Covert, D. S.; Larson, T. V.; Waggoner, A. P. *Atmos. Environ.* **1978**, *12*, 39.
(15) Chan, C. K.; Flagan, R. C.; Seinfeld, J. H. *J. Am. Ceram. Soc.* **1998**, *81*, 646.
(16) Ha, Z.; Chan, C. K. *Aerosol Sci. Technol.* **1999**, *31*, 154.
(17) Chan, C. K.; Ha, Z.; Choi, M. Y. *Atmos. Environ.* **2000**, *34*, 4795.
(18) Zhang, Y.-H.; Chan, C. K. *J. Phys. Chem. A* **2000**, *104*, 9191.
(19) Choi, M. Y.; Chan, C. K. *J. Phys. Chen. A* **2002**, *106*, 4566.
(20) Zhang, X.; Zhang, Y.; Li, Q. *J. Mol. Struct.* **2002**, *594*, 19.
(21) Martin, S. T. *Chem. Rev.* **2000**, *100*, 3403.
(22) Cziczo, D. J.; Nowak, J. B.; Hu, J. H.; Abbatt, J. P. D. *J. Geophys. Res.* **1997**, *102* (D15), 18843.
(23) (a) Zhao, L.; Zhang, Y.; Wang, L.; Cheng, H. *Chin. Sci. Bull.* **2004**, *49*, 1699. (b) Zhao, L.-J.; Zhang, Y.-H.; Wang, L.-Y.; Hu, Y.-A.; Ding, F. *Phys. Chem. Chem. Phys.* **2005**, *7*, 2723.
(24) Wei, Z.-F.; Zhang Y.-H.; Zhao, L.-J.; Liu, J.-H.; Li, X.-H. *J. Phys. Chem. A* **2005**, *109*, 1337.
(25) Rudolph, W.; Irmer, G. *J. Solution Chem.* **1994**, *23*, 663.
(26) Rudolph, W. W. *Ber. Bunsenges. Phys. Chem.* **1998**, *102*, 183.
(27) Pye, C. C.; Rudolph, W. W. *J. Phys. Chem. A* **2001**, *105*, 905.
(28) Tomišić, V.; Simeon, V. *Phys. Chem. Chem. Phys.* **2000**, *2*, 1943.
(29) Buchner, R.; Chen, T.; Hefter, G. *J. Phys. Chem. B* **2004**, *108*, 2365.
(30) Wang, F.; Zhang, Y.-H.; Li, S.-H.; Wang, L.-Y.; Zhao, L.-J. *Anal. Chem.* **2005**, *77*, 7148.
(31) Waterland, M. R.; Kelley, A. M. *J. Chem. Phys.* **2000**, *113*, 6760.
(32) Waterland, M. R.; Stockwell, D.; Kelley, A. M. *J. Chem. Phys.* **2001**, *114*, 6249.
(33) Hancer, M.; Sperline, R. P.; Miller, J. D. *Appl. Spectrosc.* **2000**, *54*, 138.
(34) Grdadolnik, J. *Acta Chim. Slov.* **2002**, *49*, 631.
(35) Zhang, Y.-H.; Chan, C. K. *J. Phys. Chem. A* **2003**, *107*, 5956.
(36) Zhang, Y.-H.; Choi, M. Y.; Chan, C. K. *J. Phys. Chem. A* **2004**, *108*, 1712.
(37) Chaban, G. M.; Huo, W. M.; Lee, T. J. *J. Chem. Phys.* **2002**, *117*, 2532.
(38) Pye, C. C.; Rudolph, W. W. *J. Phys. Chem. A* **1998**, *102*, 9933.
(39) Rodriguez-Cruz, S. E.; Jockusch, R. A.; Williams, E. R. *J. Am. Chem. Soc.* **1999**, *121*, 1986.
(40) Chen, Y.; Zhang, Y.-H.; Zhao, L.-J. *Phys. Chem. Chem. Phys.* **2004**, *6*, 537.
(41) Signorell, R. *Mol. Phys.* **2003**, *101*, 3385.
(42) Harvie, C. E.; Weare, J. H.; Hardie, L. A.; Eugster, H. P. *Science* **1980**, *208*, 498.
(43) Cheng, R. J. The generation of secondary marine aerosols: The crystallization of seawater droplets. In *Atmospheric Aerosols and Nucleation*; Wagner, P. E., Vali, G., Eds.; Springer-Verlag: New York, 1988; p 589.
(44) Weis, D. D.; Ewing, G. E. *J. Phys. Chem. A* **1999**, *103*, 4865.
(45) Hoffman, R. C.; Laskin, A.; Finlayson-Pitts, B. J. *J. Aerosol Sci.* **2004**, *35*, 869.
(46) Tang, I. N.; Fung, K. H. *J. Chem. Phys.* **1997**, *106*, 1653.